Adsorbate-Induced Segregation in the Ni{111}/Au/(*R*,*R*)-Tartaric Acid System

Timothy E. Jones,[†] Timothy C. Q. Noakes,[‡] Paul Bailey,[‡] and Christopher J. Baddeley*[,†]

School of Chemistry, University of St. Andrews, St. Andrews, Fife, KY16 9ST, United Kingdom, and MEIS Facility, CLRC Daresbury Laboratory, Warrington, Cheshire, WA4 4AD, United Kingdom

Received: August 19, 2003; In Final Form: February 12, 2004

The adsorption of the catalytically important chiral modifier, (*R*,*R*)-tartaric acid, was investigated on bimetallic Ni/Au surfaces created by annealing thin Au films on Ni{111}. Reflection adsorption infrared spectroscopy measurements revealed that the adsorption mode of (*R*,*R*)-tartaric acid depends very strongly on the surface composition. Deprotonation to produce an adsorbed bitartrate species was achieved only when small Ni clusters became available in the bimetallic surface. Medium-energy ion-scattering studies showed that, once the bitartrate species was able to be produced, significant adsorbate-induced Ni segregation was observed. Scanning tunneling microscopy (STM) investigations suggest that segregation is particularly facile in the proximity of step edges. In addition, STM revealed that the ordered (9×9) structure previously reported by Jacobsen et al.[1] is stable even with relatively high concentrations of Ni in the surface layer.

Introduction

Bimetallic Catalysis. There are many examples where bimetallic catalysts are known to outperform their monometallic counterparts.[2,3] The modification of catalytic performance has often been ascribed to either structural effects, where ensembles of active metal atoms are disrupted by the presence of the second element, or electronic effects, where the density of electronic states in the vicinity of an atom is modified by the presence of a second element. The use of Au as a second element is well known in heterogeneous catalysis. This relatively inert element has been used to dilute the activity of other elements to alter the selectivity of a catalytic reaction. For example, Ni/Au catalysts showed enhanced resistance to carbon formation in the steam-reforming process when compared with monometallic Ni catalysts.[4,5]

Enantioselective Heterogeneous Catalysis. This study forms an important part of a larger project aimed at the creation of ultraselective enantioselective Ni/Au catalysts. The Ni-catalyzed enantioselective hydrogenation of β-keto esters is one of very few examples of successful enantioselective heterogeneous catalytic reactions (ref 6 and refs therein). When Ni catalysts are modified by the adsorption of α-hydroxy acids (e.g., (*R*,*R*)-tartaric acid) or α-amino acids (e.g., (*S*)-alanine), the hydrogenation of β-ketoesters occurs enantioselectively (see Figure 1). One of the factors limiting the ultimate enantioselectivity of the catalytic reaction is the fact that bare (unmodified) Ni sites can catalyze the reaction with a comparable rate to the enantioselective reaction. Large numbers of chiral kink sites exist on metallic nanoparticles. Such sites may themselves selectively catalyze the formation of one enantiomeric product. However, statistically the kink sites of opposite handedness are predicted to exist with equal probability. Hence one would expect a racemic mixture of products from an unmodified metal catalyst. The aim of this project is to quench the reactivity of the Ni catalysts by alloying with Au. Furthermore, we predict

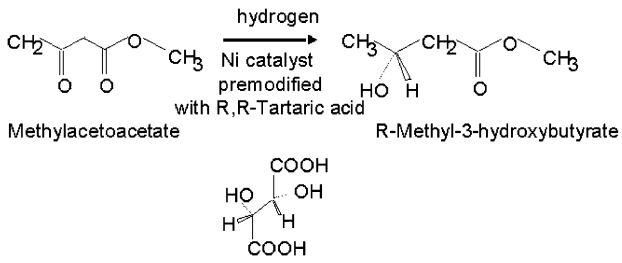

Figure 1. Reaction scheme of the Ni-catalyzed enantioselective β-ketoester hydrogenation reaction.

that the increased affinity of carboxylic acids for Ni relative to Au will result in Ni being preferentially segregated to the metal surface by the chiral modifiers. Thus, we aim to utilize the phenomenon of adsorbate-induced segregation to create Ni-rich (and hence catalytically active) chirally modified regions of the catalyst surface separated by Au-rich, catalytically inactive, unmodified regions of catalyst surface.

The Au/Ni Bimetallic System. The bulk Au/Ni phase diagram exhibits a large miscibility gap, suggesting that no alloy should be formed at low temperature.[7] However, in both the Ni{111}/Au and Ni{110}/Au systems, scanning tunneling microscopy (STM),[1,8] low-energy electron diffraction (LEED), low-energy ion-scattering,[9] and theoretical calculations[1,8,10] have confirmed that a surface alloy restricted to the outermost layer is energetically favorable.

Adsorbate-Induced Segregation. The phenomenon of adsorbate-induced segregation is one which is well known in bimetallic systems. The driving force for segregation is thought to be related both to the relative enthalpies of adsorption of the adsorbate with each elemental component of the bimetallic system and to the relative surface free energies of the two metals.[11] Additionally, there are kinetic (diffusion) barriers that need to be overcome to reach an equilibrium surface composition.[12] However, due to the fact that it is difficult to quantify with most surface analytical techniques, it is a phenomenon that is often ignored. Building on the approach first reported by Deckers et al.,[13] investigating O-induced segregation

* Author to whom correspondence should be addressed. E-mail: cjb14@st-and.ac.uk.
[†] University of St. Andrews.
[‡] CLRC Daresbury Laboratory.

10.1021/jp0364607 CCC: $27.50
Published on Web 03/19/2004

in the PtNi{111} system, we have developed a quantitative method for determining the layer-by-layer composition of bimetallic surfaces under the influence of complex adsorbates using the technique of medium-energy ion scattering (MEIS).[14] Until now, we have focused on monitoring this phenomenon on the surface of a bulk alloy single-crystal CuPd{110}.[14−16]

In this work, we report the adsorption of (*R*,*R*)-tartaric acid on Ni{111}/Au surfaces created by the deposition of Au onto Ni{111} and subsequent thermal processing. By use of reflection adsoprtion infrared spectroscopy (RAIRS), we monitor the adsorption mode of (*R*,*R*)-tartaric acid as a function of the nature of the underlying bimetallic surface. In addition, using STM, we investigate the structure of the bimetallic surfaces before and after the adsorption of (*R*,*R*)-tartaric acid. Furthermore, MEIS is used to probe the surface composition as a function of preannealing temperature and the presence or absence of the chiral modifier.

Experimental Section

Three ultrahigh vacuum (UHV) systems were used in this study. The first chamber has a base pressure of $\sim 3 \times 10^{-10}$ mbar and was built by PSP Vacuum Technology Ltd. This chamber has facilities for argon ion sputtering, a quadrupole mass spectrometer for temperature-programmed desorption (TPD) experiments and a 4-grid RFA for LEED and AES experiments.

The second chamber is an Omicron variable temperature-STM (base pressure 1×10^{-10} mbar) which, in addition to STM, has facilities for sample cleaning and LEED/AES experiments. Interfaced to this UHV system is an auxiliary chamber for RAIRS experiments using a Nicolet Nexus spectrometer with a mercury cadmium telluride detector. A typical experiment would involve the characterization of the adsorbate with RAIRS followed by UHV sample transfer for STM measurements.

The third UHV system is the CLRC MEIS facility at Daresbury Laboratory, UK.[17] This facility comprises an ion source and accelerator capable of producing H^+ or He^+ ions at energies up to 400 keV (in our case 100 keV He^+ ions), a beamline for transport of the ions with a well-defined energy ($<0.1\%$) and low angular divergence ($<0.1°$) and a multichamber UHV end station. The end station consists of a scattering chamber, a sample preparation and characterization chamber, a sample transfer system, and a fast-entry load lock. The preparation chamber is used for sample cleaning and characterization (LEED/AES).

The scattering chamber contains a precision six-axis goniometer to allow accurate alignment with the beam and a toroidal electrostatic energy analyzer with position-sensitive detector to measure the scattered-ion intensities as functions of scattering angle and ion energy. The detector system produces two-dimensional intensity maps of the ion intensity over a 1.8% range of pass energy and a scattering angle range of 24° with a resolution of 0.3% and 0.3° respectively. Full two-dimensional data sets are accumulated by taking a series of "tiles" that cover the required angle/energy range and joining them together electronically to produce a single scattered ion intensity map. While two-dimensional data sets provide a complete picture of the scattering behavior, it is normal to process the data by integrating over a range of angles or energies to produce one-dimensional plots. Angle vs scattered-ion intensity plots give structural information that can be used to calculate parameters such as surface-layer relaxation and to verify the alignment of the sample with respect to the beam. Energy spectra can be used to obtain quantitative compositional information, and a number of these plots are presented in this paper.

In each case, the Ni{111} sample was cleaned by cycles of sputtering (Ar^+, 1.5 keV) and annealing to 1000 K until a sharp (1×1) LEED pattern was obtained and no impurities were observed by AES. In each chamber, Au deposition was achieved via a resistively heated Au droplet. Initial deposition rate calibrations were carried out via Auger measurements monitoring the attenuation of the Ni (848 eV) Auger signal. The Ni{111}/Au surfaces were annealed to a specified temperature, cooled to room temperature, and then exposed to (*R*,*R*)-tartaric acid deposited via sublimation from a solid doser.

Results

1. STM/LEED. *Ni{111}/Au.* The initial growth of Au on Ni{111} was of a dendritic nature nucleated at step edges as shown in Figure 2a. Au deposition was continued until coverages of between 2 and 3 monolayers (ML) Au were achieved at a sample temperature of 300 K. Following thermal processing to 525 K, the Au islands were observed to exhibit sharp, well-defined edges, and a superstructure was formed across the whole surface (Figure 2b). Upon annealing the sample to 700 K, a Moiré structure, giving a (9×9) LEED pattern, was observed (Figure 2c) similar to that previously reported by Jacobsen et al. for Ni{111}/1.0 ML Au[1]. At higher annealing temperatures ($\sim$800 K), a similar (though sharper) LEED pattern was observed. The STM images corresponding to this surface showed a periodic array of triangular features (Figure 2d). A similar structure has also previously been reported by Jacobsen et al.[1] Following an anneal to 850 K, Figure 2e showed that, between the triangular structures, isolated bright features are observed whose height was measured to be $\sim$0.2 Å above the rest of the surface layer. In addition, a significant increase becomes apparent in the number of defects in the (9×9) structure.

Ni{111}/Au/(R,R)-Tartaric Acid. Two-dimensionally ordered structures such as those observed on Cu{110}[18] and Ni{111}[19] were never observed following (*R*,*R*)-tartaric acid adsorption on Ni{111}/Au surfaces. However, following an anneal to 800 K, the adsorption of (*R*,*R*)-tartaric acid appeared to modify the step edges of the bimetallic surface (Figure 3a). In the STM image in Figure 3a, several terraces are observed separated by double steps (see line profile in Figure 3a). The upper terrace appears to be corroded to reveal the underlying layer. At this and higher temperatures, it was also possible to image what appeared to be molecular features nucleating in these narrow step-edge regions (Figure 3b). We are not able to establish whether these species are the only tartaric acid molecules adsorbed on the surface. However, the fact that we are able to image these species may indicate that their diffusion is much more restricted than is the case for molecular species adsorbed in the centers of terraces.

2. RAIRS. RAIRS data were acquired as functions of (*R*,*R*)-tartaric acid exposure on a range of surfaces prepared by the deposition of 3 ML Au at 300 K and subsequent thermal processing. Figure 4 shows the RAIRS data following a 15-min exposure to (*R*,*R*)-tartaric acid for each bimetallic surface at a sample temperature of 300 K. The bands observed are summarized in Table 1 and are compared to the IR bands observed for solid (R,R)-tartaric acid. It is clear that, for preannealing temperatures up to 700 K, the adsorbed species resembles molecular (*R*,*R*)-tartaric acid. This spectrum is very

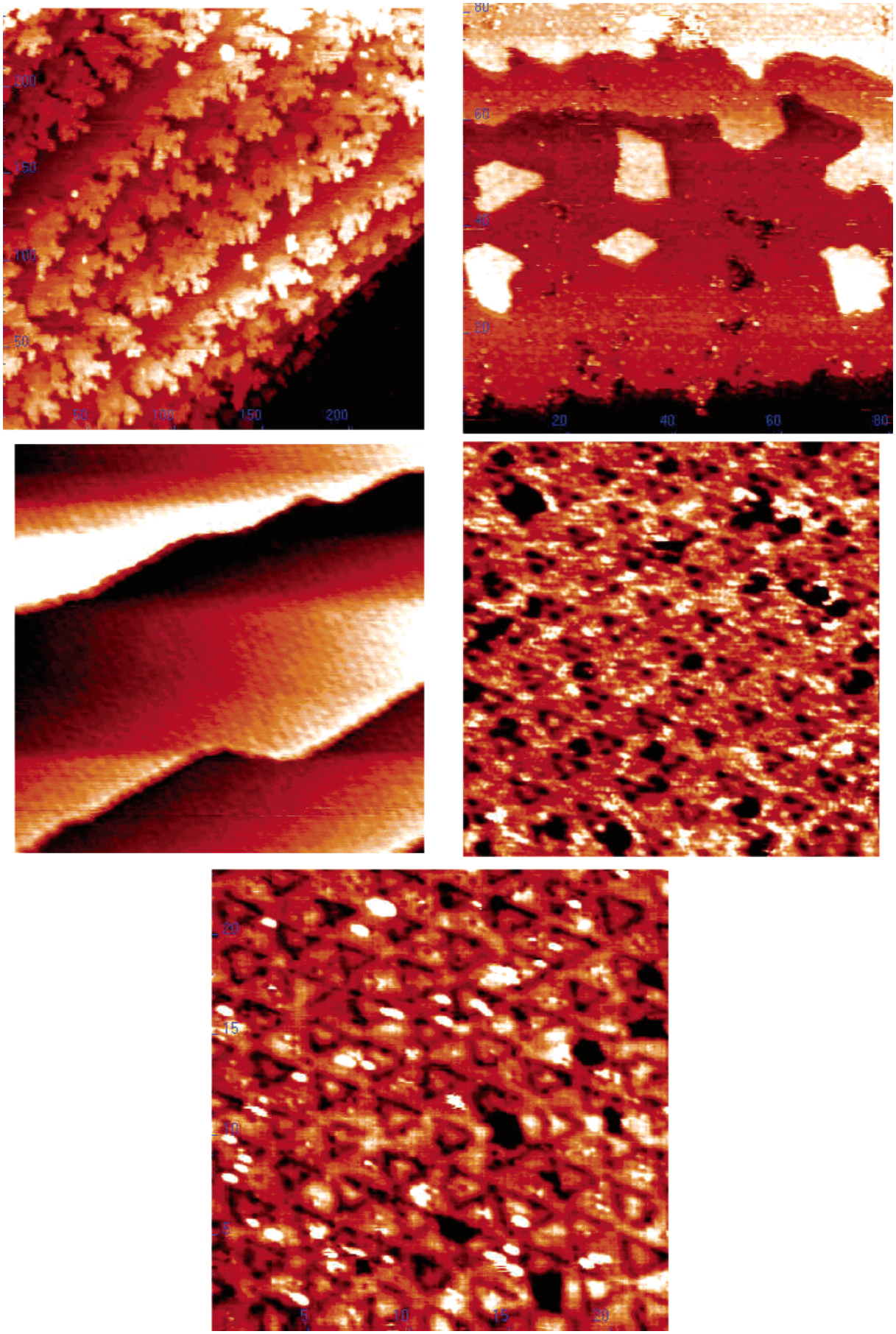

Figure 2. STM images of surfaces created by the deposition of 3 ML Au on Ni{111} at (a) 300 K (2500 × 2500 Å^2, −0.4 V, 5.2 nA) and subsequently annealed to (b) 500 K (800 × 800 Å^2, −0.6 V, 8.0 nA), (c) 700 K (850 × 850 Å^2, −0.3 V, 4.2 nA), (d) 800 K (200 × 200 Å^2, −0.3 V, 0.6 nA), and (e) 850 K (160 × 160 Å^2, −0.1 V, 0.4 nA).

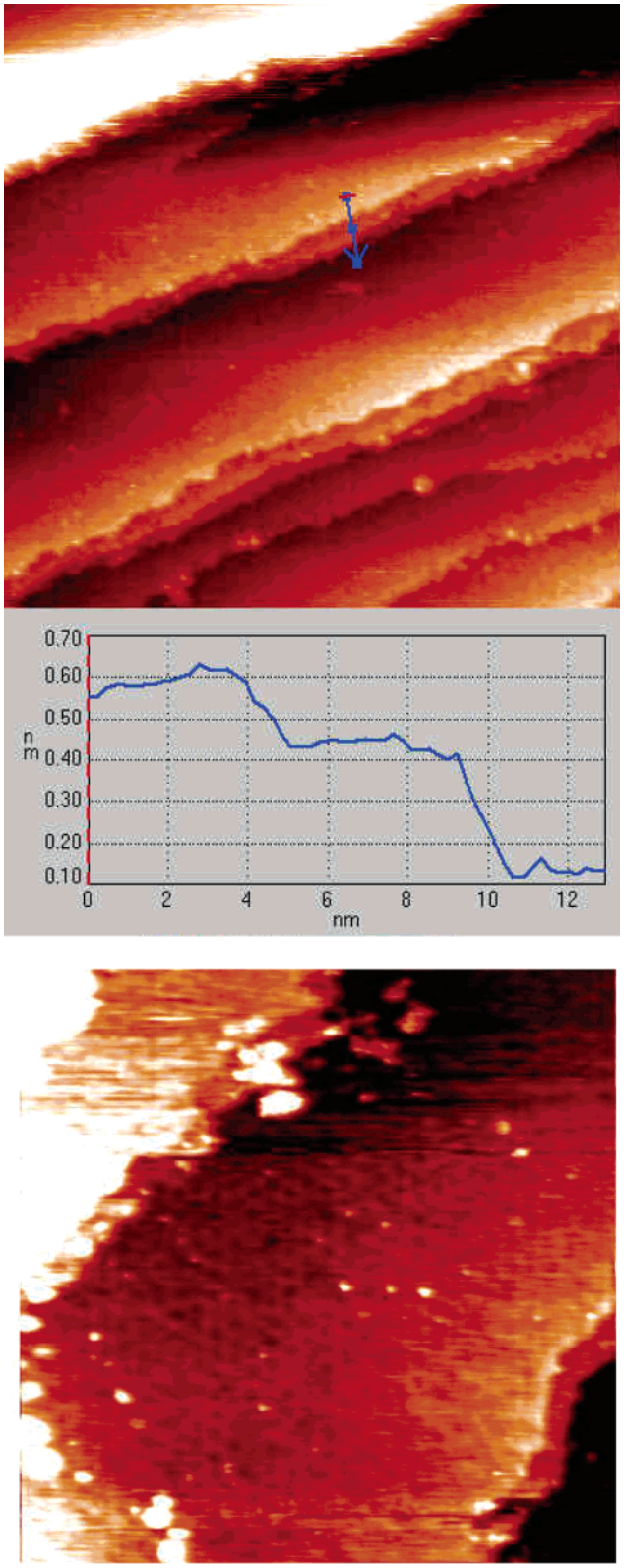

Figure 3. STM images following the adsorption of (*R*,*R*)-tartaric acid onto the surfaces shown in Figure 2d: (a) (1500 × 1500 Å^2, −0.1 V, 0.6 nA) and (b) (750 × 750 Å^2, −1.82 V, 0.2 nA).

similar to that observed following (*R*,*R*)-tartaric acid adsorption on Cu{110} at 170 K.[18] The 600 K annealed sample shows an additional feature at 2039 cm^{-1} corresponding to linear CO adsorption. Thermal processing at 800 K and above followed by (*R*,*R*)-tartaric acid exposure results in a quite different RAIR spectrum. The band at 1739 cm^{-1} is strongly attenuated, and bands at 1420 and 1589 cm^{-1} are observed, which are characteristic, respectively, of the symmetric and asymmetric stretching frequencies of carboxylate groups.

3. MEIS. MEIS data were taken from a sample consisting of 1.5 ML Au grown on Ni{111} following thermal processing to a series of annealing temperatures. The incident and exit geometries employed are shown schematically in Figure 5. At the ion beam energies employed in MEIS (100 keV He^+), the Coulombic interaction of the ion beam with the target atoms is such that the beam is able to penetrate many atomic layers into the bulk of the material. Consequently, all atoms in the top 3 layers of the idealized surface represented in Figure 5 are visible to the incoming beam. In the three exit directions shown in Figure 5, ions scattered from subsurface atoms are prevented from reaching the detector by the presence of atoms in higher-lying layers. It is these phenomena of shadowing and blocking that enable, to a first approximation, the detection of ions scattered exclusively from the top layer, the top two layers, or the top three layers of the crystalline sample. In our earlier studies of the CuPd{110} system[14−16] and the Ni{111}/Mo system,[20] we were able to take advantage of the fact that the surface alloys adopted approximately the same structure as the bulk of the sample. In the present case, a comparison of the bulk lattice parameter of Au (4.086 Å) with that of Ni (bulk lattice parameter, 3.524 Å) reveals a 15.9% mismatch, making it extremely unlikely that Au would form a pseudomorphic monolayer on Ni{111}, which has indeed been previously reported.[1,21] Hence the layer-specific geometries (which apply to the Ni bulk) are unlikely to provide quantitative information on the layer-by-layer composition in this case. However, by utilizing the fact that the detected scattered ions lose energy proportional to the depth they have penetrated into the sample, it is possible to monitor two important features of the bimetallic surface. First, one can readily ascertain whether Ni is buried beneath Au or is contained in the surface layer. Second, one can examine the blocking patterns associated with near-surface Au and Ni and compare these with bulk Ni in order to ascertain how the structure of the near-surface region compares with the bulk structure of the Ni single crystal.

Figure 6 shows the variation in position and intensity of the Ni- and Au-related features as a function of annealing temperature for a nominally 3-layer incident geometry along an outgoing 1-layer blocking direction. Following Au deposition, the Au-related feature consists of a large peak at high energy with a broad shoulder at lower energy. As the sample is annealed to subsequently higher temperatures, the shoulder gradually disappears, while the main peak loses intensity before almost completely disappearing following an annealing treatment to 1000 K. Following Au deposition, the Ni-related peak is weak in intensity and broad. There is little or no intensity at the energy corresponding to the position where the surface Ni feature would be expected. As the sample is annealed to higher temperature, the Ni feature increases in intensity and begins to resemble the corresponding feature for the clean Ni surface in both intensity and position.

Since (*R*,*R*)-tartaric acid is made up of relatively light C, H, and O atoms and since the adsorption sites of these atoms are unlikely to be sites equivalent to bulk Ni lattice sites extrapolated above the surface, the molecular adsorbate can be considered to have a negligible effect on the visibility of the underlying atoms of the metal surface to the 100 keV ion beam. This was shown to be the case in a systematic study of the effect of Cl adsorption on the visibility of the surface layers in the CuPd{110} system.[14]

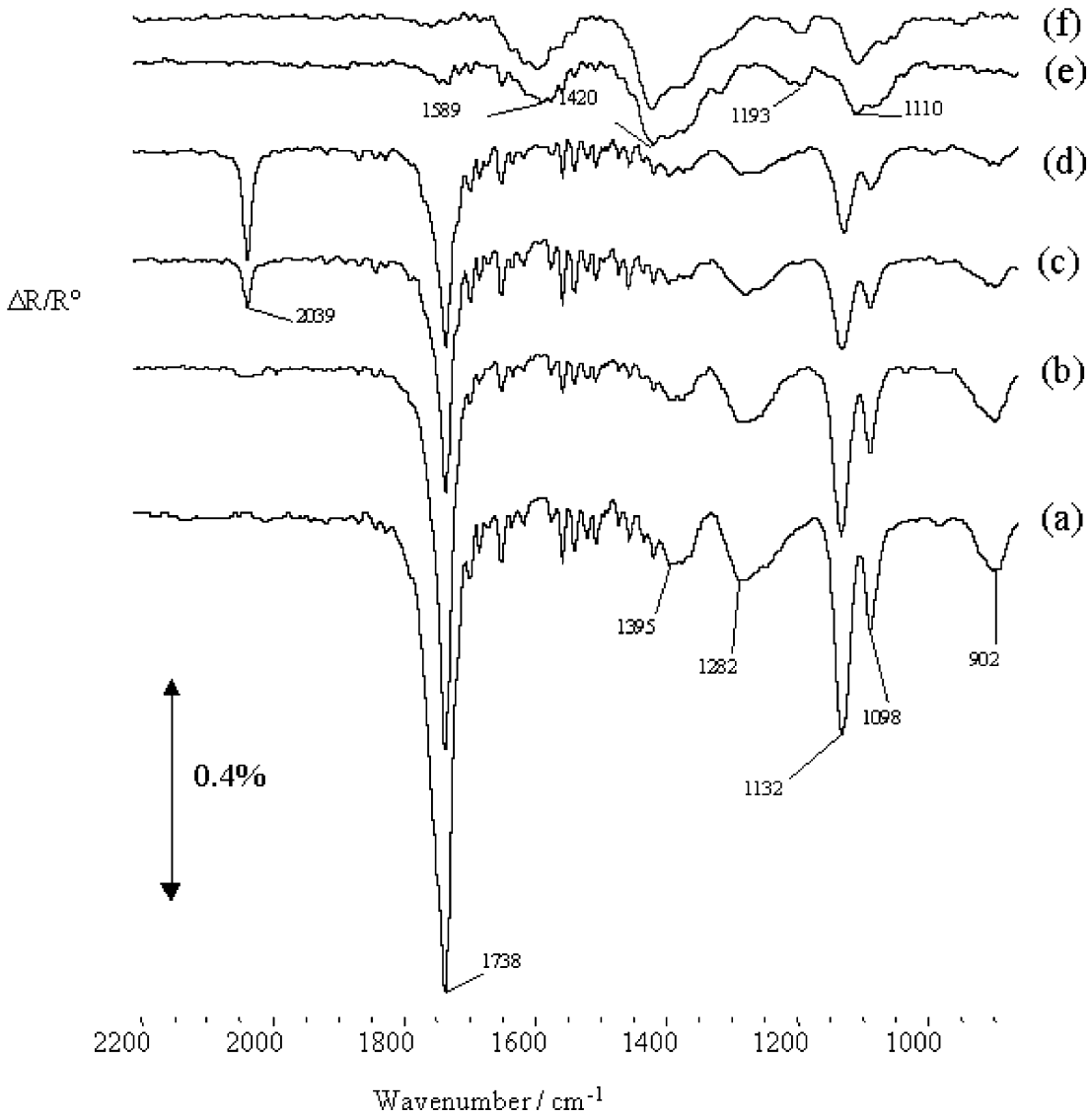

Figure 4. RAIRS data following a 15-min saturation dose of (*R*,*R*)-tartaric acid at 300 K onto a surface created by deposition of 3 ML Au on Ni{111} at 300 K and subsequently annealed to (a) 400 K, (b) 500 K, (c) 600 K, (d) 700 K, (e) 850 K, and (f) 900 K.

Ni{111}/Au/(R,R)-Tartaric Acid. We are interested to what extent the surface composition is altered by the adsorption of (*R*,*R*)-tartaric acid. On a qualitative level, we can gain some idea of the effect of (*R*,*R*)-tartaric acid by examining the relative intensities of the Ni and Au features in the MEIS intensity vs energy plots. In Figure 7, it can clearly be seen that the adsorption of (*R*,*R*)-tartaric acid onto a Ni{111}/Au preannealed to 950 K results in a significant attenuation of the Au signal. A similarly dramatic effect on the Au signal was observed following an anneal to 1000 K. A detailed study dealing with the quantitative analysis of near surface composition and structure will be reported elsewhere. In this case, by normalizing the peak intensities by dividing by the square of the atomic number (to take into account the atomic number dependence of the scattering cross section), we are able to compare the visible mole fraction of Ni and Au in the nominal 1-layer geometry before and after exposure to (*R*,*R*)-tartaric acid. Table 2 shows that, in the annealing temperature range up to 675 K, there is no obvious trend in adsorbate-induced segregation. However, upon annealing to 950 K and above, it is consistently the case that the adsorption of (*R*,*R*)-tartaric acid results in a decrease in the amount of Au visible in the nominal 1-layer geometry (i.e., at the scattering angle corresponding to the 1-layer blocking direction shown in Figure 5).

Discussion

The STM and RAIRS experiments were carried out on the same sample. The MEIS measurements were undertaken on a sample covered by slightly less Au (~1.5 ML (MEIS) and 2−3 ML (STM/RAIRS)). We have found that the thicker the Au film, the higher the annealing temperature required to obtain a given surface composition. Hence the temperature at which processes are observed in the MEIS experiments can be correlated with a slightly higher thermal treatment in the STM/RAIRS experiments.

The model proposed by Jacobsen and co-workers for the structure of the Ni{111}/Au interface involves the formation of two subtly different structures.[1] The first structure is stable at relatively low temperatures and consists of a Au monolayer on unreconstructed Ni{111}. The Au−Au spacing is thought to be slightly contracted with respect to the bulk (2.80 vs 2.89 Å) such that 8 Au−Au spacings are equivalent to 9 Ni−Ni nearest-neighbor spacings (2.49 Å). A second structure is formed at higher temperatures which is thought to consist of a Au

TABLE 1: Assignments of Bands Observed in RAIRS Experiments and a Comparison of These Data with the IR Bands Observed for (*R*,*R*)-Tartaric Acid Powder

	anneal + (*R*,*R*)-tartaric acid		Ni{111}/	
assignment	low temp	high temp	(*R*,*R*)-tartaric acid (ref 19)	(*R*,*R*)-tartaric acid powder
$\nu(OH)^{alc}$				3388
				3315
$\nu(OH)^{acid}$				3193
				3083
$\nu(CH)$				2972
				2939
$\nu(CO)^{atop}$	2039			
$\nu(C{=}O)^{acid}$	1738		1762	1741
$\nu_{asym}(OCO)$		1589		
$\nu_{sym}(OCO)$		1420	1428	
$\nu(CO)^{acid}$	1395	1395	1395	1453
$\delta(OH)^{alc}$				1375
$\delta(OH)^{alc}$ +	1282			1318
$\delta(CH)$				1255
				1220
$\delta(CH)$		1193		
$\delta(OH)^{acid}$	1132	1110	1136	
$\nu(CO)^{alc}$	1089			1190
				1134
				1089
$\nu(CC)$	902		959	992

monolayer with a similar spacing to the low-temperature structure with an underlying Ni layer, which is periodically restructured to produce misfit dislocation loops. In these regions, the second-layer Ni atoms are thought to adopt hexagonal close-packed (hcp) sites such that overlying Au atoms are able to adopt desirable 3-fold coordination sites above underlying Ni atoms. The triangular features correspond to atoms being in slightly lower positions within the monolayer than the remaining surface atoms. The face-centered cubic to hcp transition in the second layer causes a small number of Ni atoms (~5 in 81) to be removed into the surface layer to form a Au-rich alloy.[1] These Ni atoms are (at first sight surprisingly) observed as bright features.[1] This emphasizes the need to treat STM images with care, as, on the basis of atomic "size" alone, the smaller Ni atoms would be expected to appear as depressions in the image. In the present study, we observed similar bright features between the triangular features in the image. At higher annealing temperatures, these bright features were significantly more abundant than predicted on the basis of the model of Jacobsen et al.[1] In some cases, several atoms merge together to form clusters of brighter atoms. This implies that the (9 × 9) structure is stable even with a relatively high concentration of Ni in the surface layer though it may also be concluded that a greater number of defects are observed in the surface layer (Figure 2e) following this annealing treatment. We were unable to obtain high quality STM images following an anneal to 900 K, but our impression was that the (9 × 9) structure was no longer visible at this annealing temperature. Taking into account the slight difference in initial Au film thickness between STM and MEIS experiments, we may presume that the percentage of Au atoms visible in the (nominally) 1-layer geometry at such a high annealing temperature would correspond to between 10 and 20% compared with a typical value of 55% when the alloy is created. The observation with RAIRS of atop CO at annealing temperatures below that where bitartrate adsorption is observed is consistent with CO adsorption on isolated Ni atoms within the bimetallic layer.

Additionally, the RAIRS data showed some interesting effects relating to (*R*,*R*)-tartaric acid adsorption. It is not surprising that nondissociative adsorption is observed on the Au-rich surfaces.

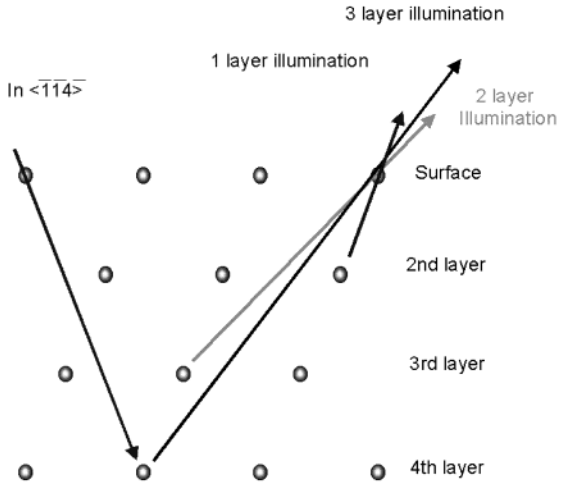

Figure 5. Schematic diagram showing the incident ion trajectories and exit directions corresponding to 1-, 2-, and 3-layer illumination along the [112] azimuth of the {111} surface.

However, it is somewhat unexpected that molecular (*R*,*R*)-tartaric acid was stable on the Au overlayer at 300 K. On Cu{110},[18] it was reported that molecular (*R*,*R*)-tartaric acid was only transiently stable on the surface at 300 K; RAIRS experiments were able to follow the decrease in the intensity of bands due to the molecular species over the course of 30 min. Indeed, TPD experiments showed that (*R*,*R*)-tartaric acid is stable on the Au surface up to ~450 K. This temperature is close to the melting point of (*R*,*R*)-tartaric acid and may reflect the fact that a structure close to the crystalline structure of (*R*,*R*)-tartaric acid is produced on the Au surface. The tendency of (*R*,*R*)-tartaric acid to deprotonate on Cu surfaces may lead to a disruption in the ability of (*R*,*R*)-tartaric acid to form such a structure on Cu and to destabilize the multilayer. Following preannealing treatments to 800 K and above, characteristic bands were observed corresponding to bitartrate formation. However, the adsorption geometry of bitartrate is markedly different to that observed on either Ni{111},[19] Ni{110},[22] or Cu{110}.[18] The presence of a pair of bands at 1596 and 1420 cm^{-1} may be assigned to the asymmetric and symmetric stretches of the carboxylate group, respectively. In the previous studies of tartrate on metal surfaces, only the 1420-cm^{-1} band was observed. By application of the IR metal surface selection rule, this was interpreted as being due to the two oxygens of the carboxylate functionality being equidistant from the surface. In such an adsorption geometry, the dynamic dipole moment associated with the symmetric stretch had a component perpendicular to the surface. By contrast, the dynamic dipole moment associated with the asymmetric stretching frequency had no component perpendicular to the surface. In the present study, the observation of both bands is strongly indicative that the bitartrate species adopts a more tilted geometry on the bimetallic surface. This may be related to the fact that molecular features are observed in the vicinity of surface steps.

The behavior at the step edges is intriguing. Parts a and b of Figure 3 appear to show that the adsorption of (*R*,*R*)-tartaric acid results in the modification of the step-edge region with the top layer being corroded and the second layer being exposed and covered by adsorbate. If the model proposed by Jacobsen et al.[1] is correct, the top layer of the bimetallic surface almost exclusively consists of Au while the second layer can be considered to be pure Ni. These data are consistent with a significant contribution to adsorbate-induced segregation involving the corrosion of step edges. It is not clear from our data

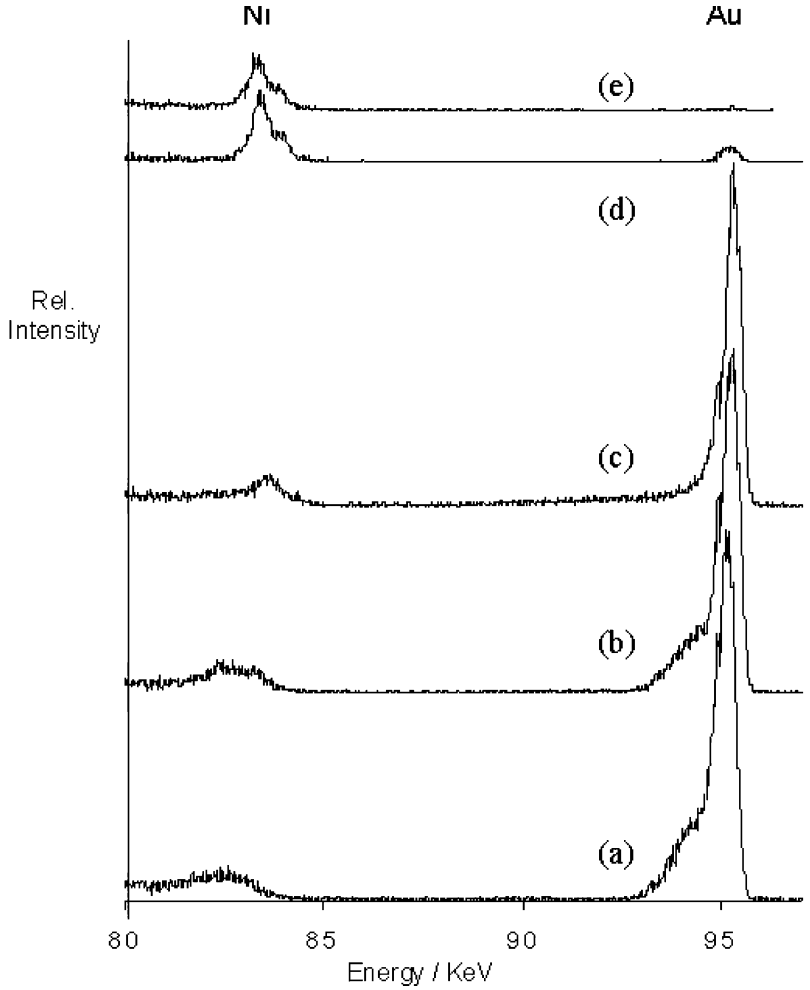

Figure 6. Ion intensity vs scattered-ion energy plots for an ~1.5 ML Au film on Ni{111} annealed to (a) 375 K, (b) 525 K, (c) 675 K, (d) 1000 K, and (e) clean Ni. Data are taken using a [114] incident direction and a [110] exit direction.

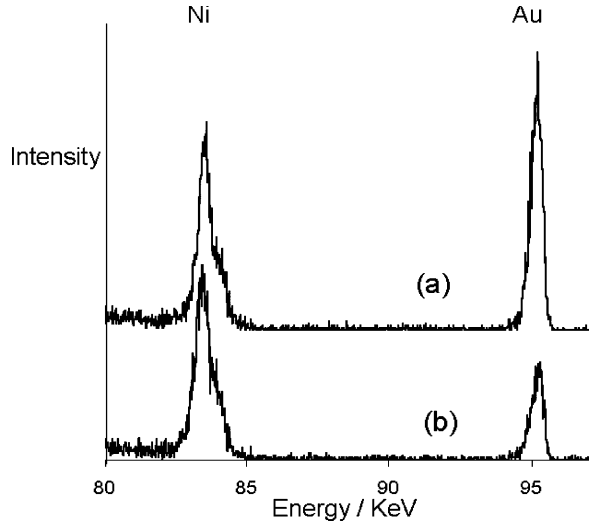

Figure 7. Ion intensity vs scattered-ion energy spectra from an ~1.5 ML Au film on Ni{111} (a) preannealed to 950 K and (b) exactly the same surface exposed to a saturation dose of (*R*,*R*)-tartaric acid at 300 K. Data are taken using a [114] incident direction and a [110] exit direction

whether a second mechanism exists whereby, once clusters of Ni are present in the terraces, adsorption of (*R*,*R*)-tartaric acid results in further segregation in the vicinity of the clusters. It is noteworthy, however, that while CO chemisorption on Ni singletons is possible, bitartrate adsorption on such sites appears not to be possible. This suggests that there must be a finite Ni cluster size for adsorbate-induced segregation to occur in the terrace regions.

TABLE 2: Mole Fraction of Au Visible in the Nominal 1-Layer Geometry before and after Exposure to (*R*,*R*)-Tartaric Acid at 300 K[a]

	atom % Au	
annealing temperature/K	before (*R*,*R*)-tartaric acid exposure	after (*R*,*R*)-tartaric acid exposure
375	55.5	54.0
525	55.3	58.9
675	51.3	50.9
875	25.5	22.0
950	11.3	4.5
1000	1.9	1.3

[a] NB the actual layer illumination is probably at least 2 layers. Each sample corresponds to a 1.5-ML Au film deposited on Ni{111} at 300 K and subsequently annealed to the temperature specified in the left-hand column.

Once again taking into account the slight differences in initial Au coverage between the STM and MEIS experiments, it can be presumed that the onset of the bitartrate conformation coincides with the sharp drop in visible Au atoms observed in MEIS experiments above 675 K.

Our MEIS experiments have demonstrated once again that this technique is extremely effective in observing effects of adsorbate-induced segregation. In this paper, we have reported qualitative compositional changes, which are clear from a

comparison of the relative intensities of the Ni and Au peaks before and after (*R*,*R*)-tartaric acid adsorption. Achieving a quantitative compositional analysis such as we have achieved before for Ni{111}/Mo[20] and CuPd{110}[14−16] is much more problematic. For example, using the experimental geometries employed in this work, VEGAS[23] simulations reveal that, for the clean Ni{111] surface, in the nominally 1-layer geometry, we would expect to illuminate 1.3−1.4 layers of the surface due to a combination of factors such as bulk and surface lattice vibrations and the surface layer relaxation. In the present study, adding 1 ML of Au in a (9 × 9) arrangement would not be expected to effectively block ions scattered from the underlying Ni layer. This explains why only ∼55% of the visible atoms are Au despite the fact that the both STM and RAIRS point to almost the entire surface being Au.

From the point of view of enantioselective catalysis, it seems highly promising that (*R*,*R*)-tartaric acid can induce Ni segregation at 300 K. If bimetallic nanoparticles could be produced that are Au rich, it is highly likely that the hydrogenation reaction would be quenched over the Au-rich regions, leaving the chirally modified regions to control the selectivity of the catalyst.

Conclusions

1. Similar (9 × 9) structures as observed by Jacobsen et al. were observed in the present structure. The stability of the (9 × 9) structure is such that a considerable number of Ni atoms can be incorporated into the surface prior to breakdown of the ordered structure.

2. (*R*,*R*)-tartaric acid adsorbs molecularly on the Au-rich surface of the (9 × 9) structure. The deprotonation of (*R*,*R*)-tartaric acid is not observed when isolated Ni atoms are present in the surface layer.

3. Once the concentration of Ni has reached a threshold level in the surface layer, (*R*,*R*)-tartaric acid chemisorption occurs with the formation of bitartrate species whose orientation with respect to the surface is quite different to that observed on either monometallic Ni or Cu surfaces.

4. (*R*,*R*)-tartaric acid chemisorption causes segregation of Ni to the surface layer at least partly due to the exposure of Ni-rich regions at step edges.

Acknowledgment. This work is supported by the Engineering and Physical Sciences Research Council (GR/R16198) in the form of a PDRA for T.E.J. and access to the MEIS facility at CLRC Daresbury Laboratory. In addition, we are very grateful to Professor Neville Richardson for access to his STM/RAIRS chamber.

References and Notes

(1) Jacobsen, J.; Nielsen, L. P.; Besenbacher, F.; Stensgaard, I.; Laegsgaard, E.; Rasmussen, T.; Jacobsen, K. W.; Nørskov, J. K. *Phys. Rev. Lett.* **1995**, *75*, 489

(2) Rao, G. R. *Curr. Sci.* **1998,** *75*, 901

(3) Sinfelt, J. H. *Acc. Chem. Res.* **1987**, *20*, 134

(4) Besenbacher, F.; Chorkendorff, I.; Clausen, B. S.; Hammer, B.; Molenbroek, A. M.; Nørskov, J. K.; Stensgaard, I. *Science* **1998**, *279*, 1913

(5) Molenbroek A. M.; Nørskov, J. K.; Clausen, B. S. *J. Phys. Chem. B* **2001**, *105*, 5450

(6) Tai, A.; Sugimura, T. *Chiral Catalyst Immobilization and Recycling*; de Vos, D. E.; Vankelecom, I. F. J.; Jacobs, P. A., Eds.; Wiley−VCH: New York, 2000; Chapter 8, pp 173−208

(7) *Binary Alloy Phase Diagrams*; Massalki, T. B., Ed.; American Society for Metals: Metals Park, Ohio, 1986

(8) Nielsen, L. P.; Besenbacher, F.; Stensgaard, I.; Laegsgaard, E.; Engdahl, C.; Stoltze, P.; Jacobsen, K. W.; Nørskov, J. K. *Phys. Rev. Lett.* **1993**, *71*, 754

(9) Boerma, D.; Dorenbos, G.; Wheatley, G. H.; Buck, T. M. *Surf. Sci.* **1994**, *307*−*309*, 674

(10) Ruban, A. V.; Skriver, H. L.; Nørskov, J. K. *Phys. Rev. B* **1999**, *59*, 15990

(11) Tománek, D.; Mukherjee, S.; Kumar, V.; Bennemann, K. H. *Surf. Sci.* **1982**, *114*, 11

(12) Hodak, J. H.; Henglein, M.; Giergsig, M.; Hartland, G. V. *J. Phys. Chem. B* **2000**, *104*, 11708

(13) Deckers, S.; Habraken, F. H. P. M.; van der Weg, W. F.; Denier van der Gon, A. W.; van der Veen, J. F.; Geus, J. W. *Appl. Surf. Sci.* **1990**, *45*, 121

(14) Baddeley, C. J.; Bloxham, L. H.; Laroze, S. C.; Raval, R.; Noakes, T. C. Q.; Bailey, P. *J. Phys. Chem. B* **2001**, *105*, 2766

(15) Noakes, T. C. Q.; Bailey, P.; Laroze, S. C.; Bloxham, L. H.; Raval, R.; Baddeley, C. J. *Surf. Interface Anal.* **2000**, *30*, 81

(16) Baddeley, C. J.; Bloxham, L. H.; Laroze, S. C.; Raval, R.; Noakes, T. C. Q.; Bailey, P. *Surf. Sci.* **1999**, *435*, 827

(17) Bailey, P.; Noakes, T. C. Q.; Woodruff, D. P. *Surf. Sci.* **1999**, *426*, 358

(18) Lorenzo, M. O.; Haq, S.; Bertrams, Th.; Murray, P. W.; Raval, R.; Baddeley, C. J. *J. Phys. Chem. B* **1999**, *103*, 10661

(19) Jones, T. E.; Baddeley, C. J. *Surf. Sci.* **2002**, *513*, 453

(20) Jones T. E.; Noakes T. C. Q.; Bailey P.; Baddeley C. J. *Surf. Sci.* **2003**, *523*, 12

(21) Umezawa, K.; Nakanishi, S.; Gibson, W. M. *Surf. Sci.* **1999**, *426*, 225

(22) Humblot, V.; Haq, S.; Muryn, C.; Hofer, W.; Raval, R. *J. Am. Chem. Soc.* **2002**, *124*, 503

(23) Frenken J. W. M.; Tromp R. M.; van der Veen J. F. *Nucl. Instrum. Methods Phys. Res., Sect. B* **1986**, *17*, 334